Electronic Supplementary Information

Boosting photocatalytic performance of $Cd_xZn_{1-x}S$ for H_2 production by Mo_2C MXene with large interlayer distance

Sen Jin,[a] Jiabin Wu,[b] Jizhou Jiang,[c] Ruige Wang,[a] Bingxin Zhou,[a] Libo Wang,[a] Qianku Hu[a] and Aiguo Zhou*[a]

[a]School of Materials Science and Engineering, Henan Polytechnic University, Jiaozuo, Henan 454003, China

[b]Department of Chemistry, Tsinghua University, Beijing 100084, China

[c]School of Environmental Ecology and Biological Engineering, Key Laboratory of Green Chemical Engineering Process of Ministry of Education, Engineering Research Center of Phosphorus Resources Development and Utilization of Ministry of Education, Wuhan Institute of Technology, Wuhan 430205, Hubei, China

*Corresponding author:

Aiguo Zhou, zhouag@hpu.edu.cn

Experiment S1

Determination of the optimal ratio of Cd and Zn in $Cd_xZn_{1-x}S$ solid solution.

4 mmol of $Cd(NO_3)_2·4H_2O$ (Macklin, Shanghai, China, AR 99%) and $Zn(NO_3)_2·6H_2O$ (Fengchuan Chemical Reagent Technology Co., LTD, Tianjin, China, AR 99%) was dissolved in 20 mL de-ionized water to form mixed cadmium and zinc source solution. Then 4 mmol of $(NH_4)_2S$ (Aladdin, Shanghai, China, AR 20% in H_2O) solution was diluted in 20 mL de-ionized water to provide sulfur source. Thereafter, the $(NH_4)_2S$ aqueous solution was added dropwise into the above mixed solution with stirring at room temperature. After 1 h chemical reaction, the precipitate was centrifuged and washed by de-ionized water and ethanol until pH≈7, followed by drying in vacuum at 60 °C overnight. At last, the block samples with different color were added successively in a mortar and grinded thoroughly using a pestle until a homogenous powder. According to molar ratio of Cd and Zn, the amount of $Cd(NO_3)_2$ and $Zn(NO_3)_2$ is based on the formula of $Cd_xZn_{1-x}S$ (x = 0.1, 0.2, 0.3, …, 0.9), and the corresponding CZS samples were labeled as $Cd_{0.1}Zn_{0.9}S$, $Cd_{0.2}Zn_{0.8}S$, $Cd_{0.3}Zn_{0.7}S$, $Cd_{0.4}Zn_{0.6}S$, $Cd_{0.5}Zn_{0.5}S$, $Cd_{0.6}Zn_{0.4}S$, $Cd_{0.7}Zn_{0.3}S$, $Cd_{0.8}Zn_{0.2}S$ and $Cd_{0.9}Zn_{0.1}S$.

Experiment S2

Physicochemical characterizations.

The component of all the samples were tested by X-ray diffraction (XRD; Smart-lab, Rigaku Corporation, Japan) using Cu-K_α (λ =1.5406 Å) radiation at a scan rate of 0.02 2θ s^{-1}. The microstructures were observed by scanning electron microscopy (SEM; Merlin Compact, Zeiss, Germany) equipped with an energy disperse spectroscope (EDS; X-MaxN, Oxford, UK) and transmission electron microscope (TEM, 2100F, JEM, Japan) with an accelerating voltage of 200 kV. The powder size distribution was tested by a particle size analyzer via wet process (Mastersizer 3000, Malvern, UK). The surface chemical element composition and chemical states of the samples were characterized by an X-ray photoelectron spectrometer (XPS, ESCALAB 250X, ThermoFischer, USA). The spectra were excited by Al K_α source (hv=1486.6 eV, operated at 12.5 kV with heater current of 16 mA) with a passing-energy of 100 eV for survey spectra and 20 eV for high-resolution spectra at a step size of 0.05 eV. The Brunauer-Emmett-Teller (BET) specific surface area (SSA) of the samples were investigated by N_2 adsorption-desorption at 77 K using a Micromeritics ASAP2460 adsorption analyzer and the SSA was determined by a multipoint BET method utilizing the adsorption data in the range of relative pressure (P/P_0) of 0.05-0.3. All the samples were pretreated by degassing at 80°C in vacuum before N_2 adsorption measurements. The ultraviolet-visible (UV-Vis) diffuse reflectance spectra were tested by dry-pressing disk samples with an ultraviolet-visible spectrophotometer (UH4150, Hitachi, Japan) and using $BaSO_4$ as the reflectance standard in the spectral range of 200-800 nm. The photoluminescence (PL) spectra were measured by a spectrofluorophotometer (Fluoromax-4, Horiba, Japan) under the excitation of 375 nm at room temperature to evaluate the ability of photogenerated carriers.

Experiment S3

Electrochemical and photoelectrochemical measurements.

Photoelectrochemical experiments were carried out by an electrochemical analyzer (Autolab RDE-2, Metrohm, Switzerland) in a standard three-electrode system using the samples as the working electrodes, Ag/AgCl as a reference electrode and the Pt wire as the counter electrode. The transient photocurrent (TPC) measurements were tested under visible light irradiation (λ≥420 nm) with on/off switches at a bias of 0.2 V (vs. Ag/AgCl). The electrochemical impedance spectra (EIS) experiments were performed at an amplitude of 0.01 V (vs. Ag/AgCl) and over the frequency ranges from 100 kHz to 0.1 Hz under visible light irradiation (λ≥420 nm). The Mott-Schottky plots were recorded over the AC frequencies of 500, 800 and 1000 Hz in the dark. The electrolyte in all the electrochemical measurements was 0.5 M Na_2SO_4 aqueous solution. Before the preparation of working electrodes, all the FTO glass plates (1 cm × 2.5 cm) were washed with acetone, de-ionized water and ethanol, respectively, by ultrasonication for 30 min. The working electrodes of Mo_2C MXene and CZS/Mo_2C samples were prepared as follows: 10 mg of as-prepared samples were dispersed in mixture (400 μL de-ionized water, 100 μL ethanol, 100 μL Nafion for MXenes and 500 μL ethanol, 100 μL Nafion for CZS/Mo_2C samples), followed by ultrasonication for 2 h to make uniform slurries. Thereafter, 100 μL of the slurry was coated onto a FTO glass plate and dried in air for whole night. The work area of the working electrode immersed in the electrolyte was 1 cm^2.

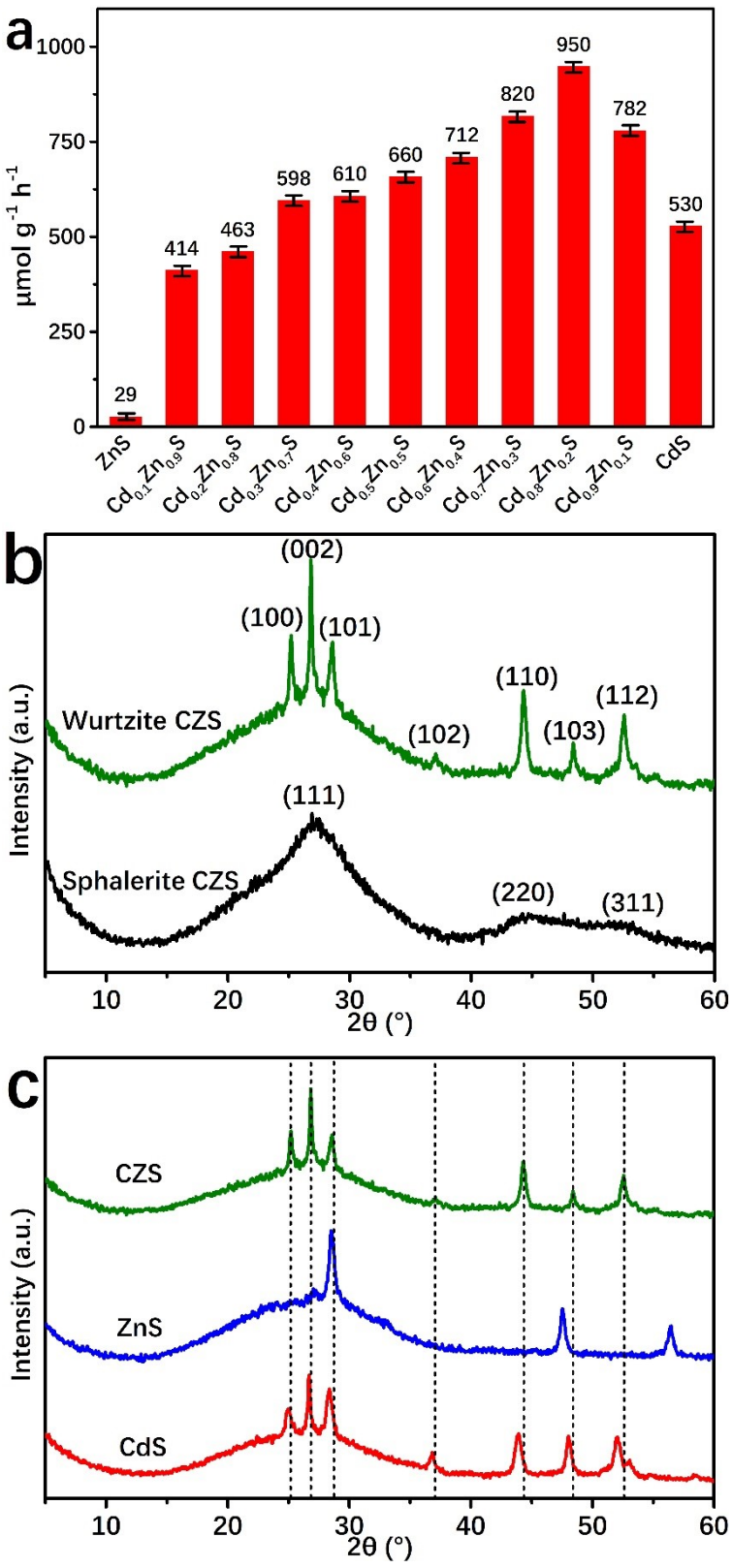

Fig. S1 (a) The photocatalytic activities of $Cd_xZn_{1-x}S$ samples before hydrothermal treatments under visible-light illumination. XRD patterns of (b) $Cd_{0.8}Zn_{0.2}S$ before (black pattern) and after (green pattern) hydrothermal treatments, (c) pure CdS, ZnS and $Cd_{0.8}Zn_{0.2}S$ after hydrothermal treatments. The dotted lines in (c) display the position of peaks of $Cd_{0.8}Zn_{0.2}S$.

As shown in Fig. S1b, the main crystal composition of $Cd_{0.8}Zn_{0.2}S$ is sphalerite phase because the starting materials are used for chemical reaction at room temperature. After hydrothermal treatment in ethylenediamine, the (111) peak of sphalerite $Cd_{0.8}Zn_{0.2}S$[1] transformed into one sharp and intense (002) peak with two shoulder peaks at 25.2 and 28.6°, which implied the highly crystalline nature. These arisen diffraction peaks, also including the peaks from 45 to 53°, distinctly reveal that the conversion of crystal phase (from sphalerite to wurtzite) can be achieved by the method mentioned in this paper. Since the Cd content in $Cd_{0.8}Zn_{0.2}S$ is dominant, compared with pure CdS synthesized in this paper after hydrothermal treatment in Fig. S1c, all the characteristic peaks of $Cd_{0.8}Zn_{0.2}S$ show a slight shift toward higher degrees with a decreased interplanar spacing, which is attributed to Zn^{2+} ions doping into CdS and the formation of solid solution.[2]

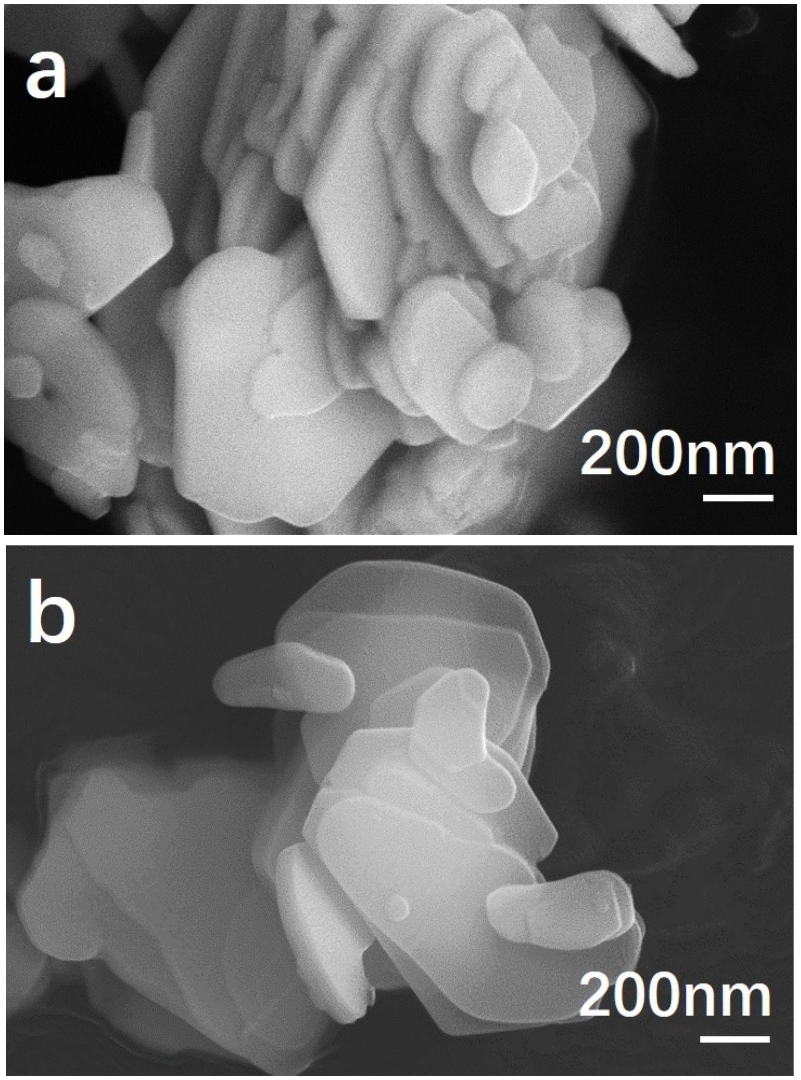

Fig. S2 SEM images of (a) raw Mo_2Ga_2C and (b) Mo_2C MXene prepared by common etching method.

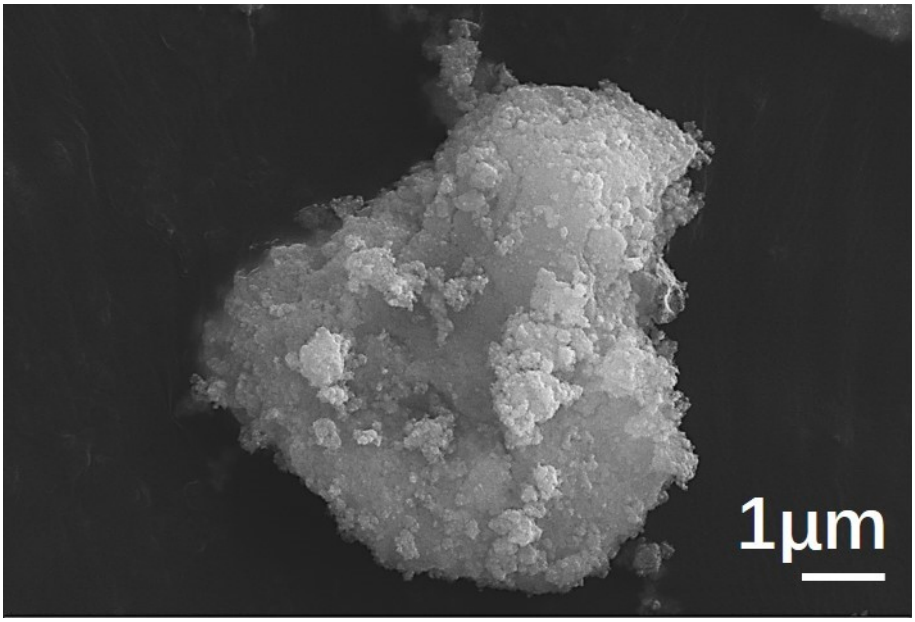

Fig. S3 SEM image of sphalerite CZSM*x* sample.

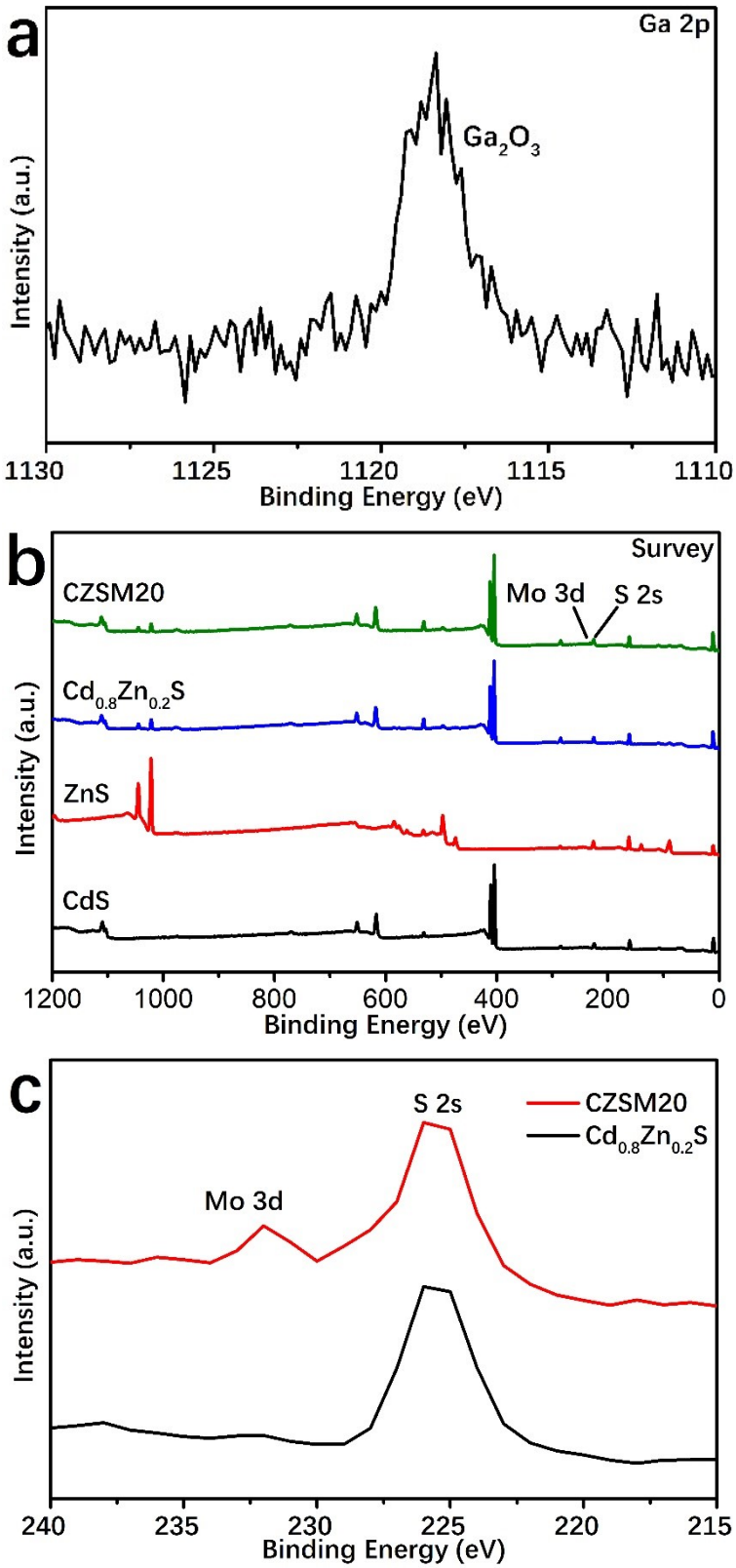

Fig. S4 (a) High resolution XPS spectrum of Ga 2p region for Mo_2C-CTAB. (b) The full-scale XPS spectra of CdS, ZnS and $Cd_{0.8}Zn_{0.2}S$ before and after coupling with Mo_2C-CTAB. (c) The survey spectra of $Cd_{0.8}Zn_{0.2}S$ and CZSM20 focusing on the binding energy range from 215 to 240 eV, showing the existence of peak of Mo 3d.

Supplementary Note 1

The discussion about the negligible existence of Ga_2O_3 in Mo_2C-CTAB.

At the beginning of synthesizing Mo_2Ga_2C, β-Mo_2C powders were mixed with molten Ga in air. The vacuum-sealing process may not be perfect during heating the starting materials at high temperature. Besides, some characterization processes, such as XRD, were also handled in air. As a result, the inevitable contacting with air leads to the generation of Ga_2O_3, thereby coexisting with Mo_2Ga_2C. Similar phenomenon can be found in the preparation of Ti_3AlC_2 with negligible Al_2O_3 impurity.[3] The formed Ga_2O_3 has more chemical stability than Ga in acid solution, resulting in incomplete removal of Ga_2O_3 during etching process. Therefore, a little Ga_2O_3 coexist with Mo_2C-CTAB during the subsequent experiments.

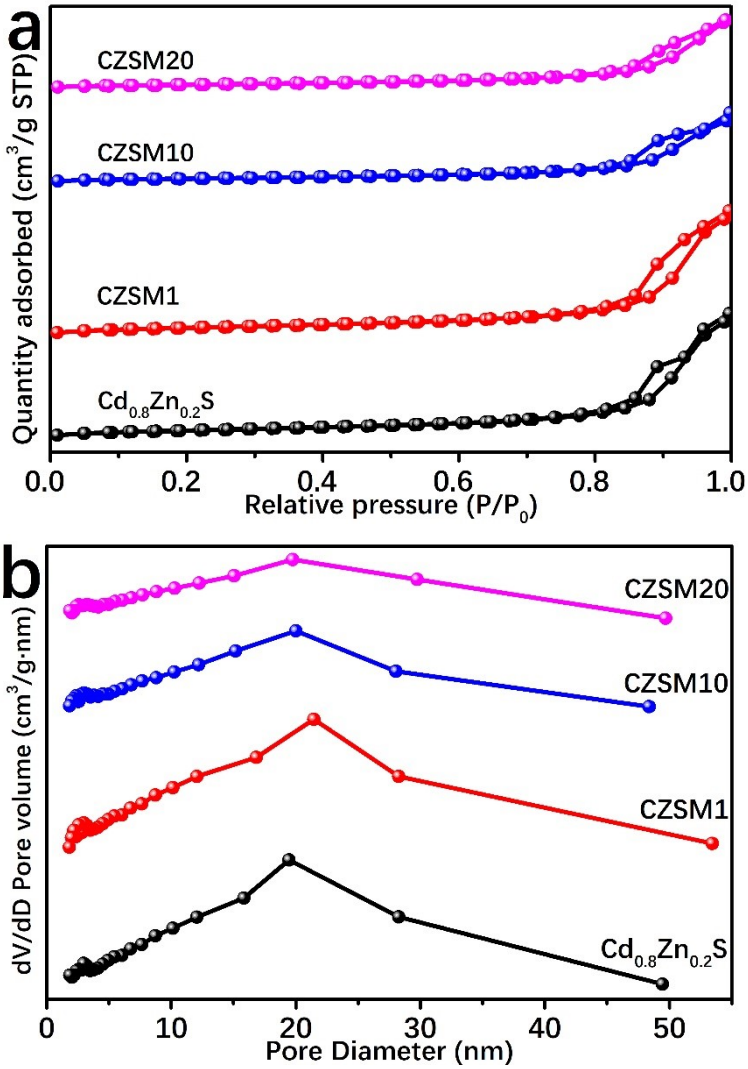

Fig. S5 N_2 adsorption-desorption isotherms (a) and pore size distribution curves (b) of $Cd_{0.8}Zn_{0.2}S$, CZSM1, CZSM10 and CZSM20.

Tab. S1 SSA, pore volume and average pore diameter of samples.

Samples	SSA (m^2 g^{-1})	Pore Volume (cm^3 g^{-1})	Average pore diameter (nm)
$Cd_{0.8}Zn_{0.2}S$	45.5	0.18	17.0
CZSM1	45.1	0.18	16.9
CZSM2.5	40.0	0.16	17.9
CZSM5	40.7	0.15	16.7
CZSM10	37.6	0.15	16.4
CZSM15	40.6	0.16	15.7
CZSM20	38.2	0.15	16.9
CZSM25	38.0	0.15	16.0

Tab. S2 Comparison of AQE values of samples.

Samples	AQE values (%)
$Cd_{0.8}Zn_{0.2}S$	2.5
CZSM1	9.1
CZSM2.5	10.3
CZSM5	13.8
CZSM10	15.6
CZSM15	19.8
CZSM20	22.5
CZSM25	20.6

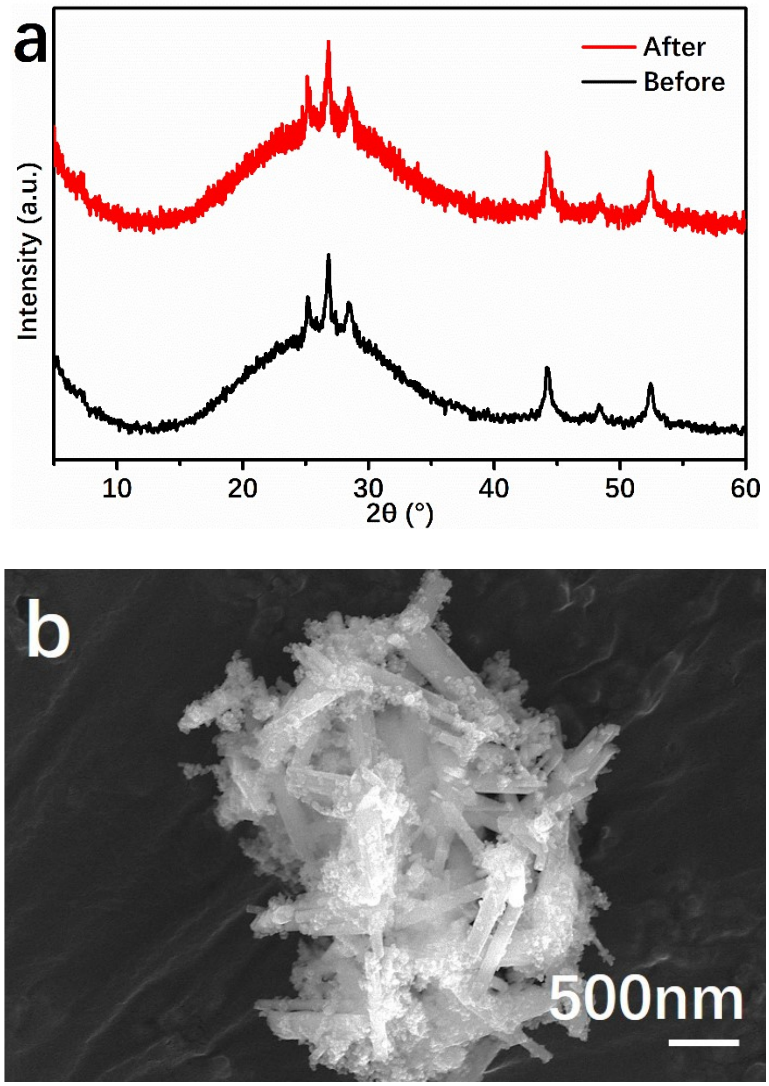

Fig. S6 (a) XRD patterns of CZSM20 before and after cycling tests. (b) SEM image of CZSM20 after cycling test.

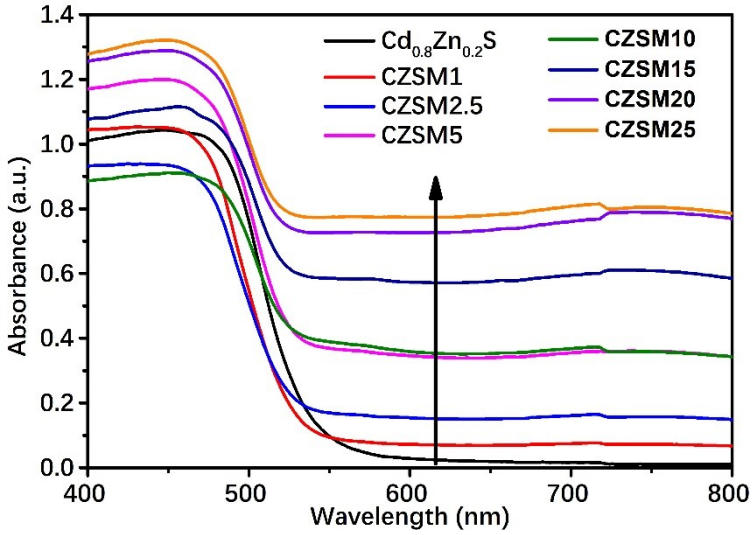

Fig. S7 The UV-Vis diffuse reflectance spectra of CZSM*x* samples.

Tab. S3 Comparison of PL decay time (τ) and the corresponding relative amplitude (f) of $Cd_{0.8}Zn_{0.2}S$ and CZSM20 tested by time-resolved PL spectroscopy.

Samples	**Decay time (ns)**		**Relative amplitude (%)**		**Average lifetime (τ, ns)***	χ^2
	τ_1	τ_2	f_1	f_2		
$Cd_{0.8}Zn_{0.2}S$	1.0457	5.4716	39.15	60.85	3.73	1.2832
CZSM20	1.9630	8.1575	47.02	52.98	5.24	1.2277

* The average lifetime of carriers is calculated by the equation: $\tau = \tau_1 f_1 + \tau_2 f_2$

χ^2: The goodness of fit parameter.

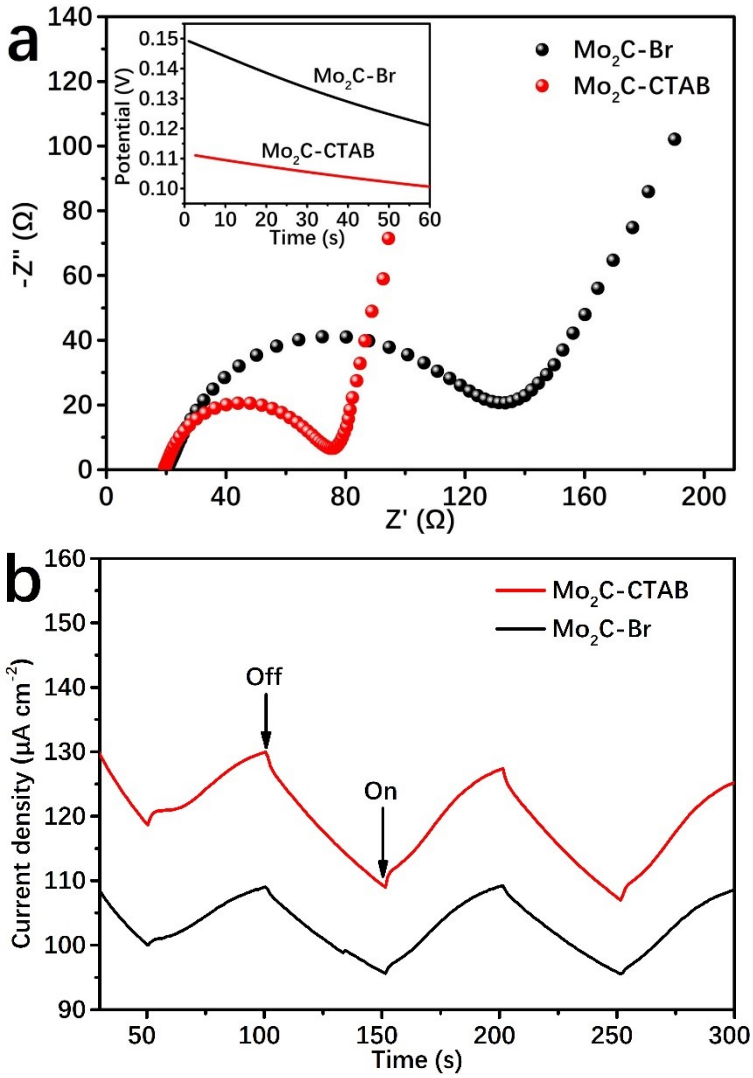

Fig. S8 Nyquist plots (a) and TPC responses (b) of Mo_2C-CTAB and Mo_2C-Br. The inset in (a) is their OCP versus time curves.

Supplementary Note 2

Analysis of photoelectrodes kinetic properties of MXenes.

EIS was used to check the kinetic properties of Mo_2C-CTAB and Mo_2C-Br on as-prepared photoelectrodes over different frequency of AC voltage. Fig. S7a compares the Nyquist plots of two MXenes as electrode materials. The two plots are composed of a semicircle with large curvature in high and medium frequency regions, while a linear tendency in low frequency regions. It can be seen clearly that Mo_2C-CTAB has a smaller diameter of semicircle than that of Mo_2C-Br, which distinctly reveals that Mo_2C MXene etched by CTAB possesses better charge-transfer efficiency with weak transfer impedance as compared to Mo_2C MXene prepared by NH_4Br. In general, the changing process of open circuit potential (OCP) versus time reflects the status of the electrode from instability to stability. From the OCP curves in the inset (Fig. S7a), Mo_2C-CTAB has a smaller slope, indicating the photoelectrode of Mo_2C-CTAB can faster achieve the stability in the same time and the variation range of OCP value of Mo_2C-CTAB is smaller. The Warburg impedance,[4] displayed in the low frequency region, can reflects the solid-state diffusion ability of carriers in the bulk materials. As shown in Fig. S7a, the Mo_2C-CTAB photoelectrode exhibits a Warburg impedance that is almost perpendicular to the x axis, suggesting that the interlayer spacing of Mo_2C flakes connected by CTA^+ is beneficial to the diffusion and transfer of photongenerated carriers between the layers.

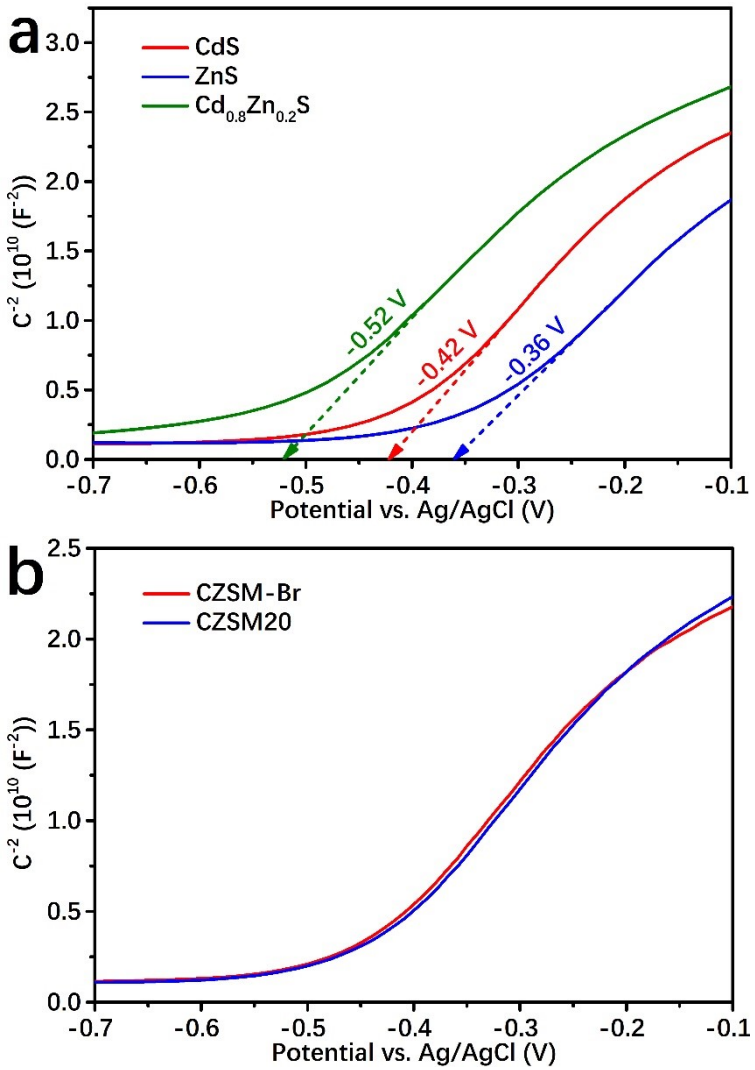

Fig. S9 Mott-Schottky plots of: (a) pure CdS, ZnS and $Cd_{0.8}Zn_{0.2}S$, (b) CZSM20 and CZSM-Br. All these Mott-Schottky values were tested over AC frequency of 1000 Hz.

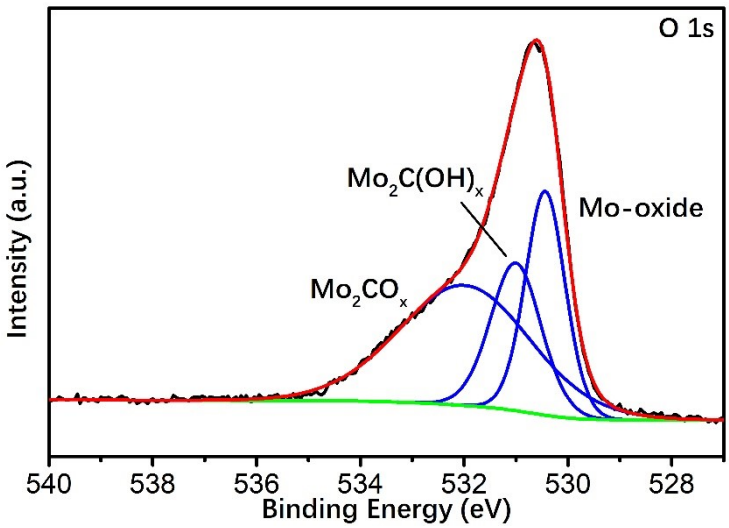

Fig. S10 The XPS spectrum of Mo_2C-CTAB for O 1s.

Supplementary Note 3

Discussion of the Fermi level of Mo_2C-CTAB.

According to the previous theoretical calculation,[5] the Fermi level of O-terminated Mo_2C MXene is calculated to be 1.09 V vs. NHE. To check the -O content on the surface of Mo_2C-CTAB, the high-resolution XPS spectrum in O 1s region was tested and shown in Fig. S10. The peaks at 531.0 and 532.0 eV can be assigned, respectively, to $Mo_2C(OH)_x$ (OH-termination) and Mo_2CO_x (O-termination).[6] It is worth noting that only ~20 at.% of -OH species in O 1s region was detected, indicating most O-terminations was converted from OH-terminations by losing the H^+ during etching process and more CTA^+ could be adsorbed in the interlayer spacing. Thus O-terminated Mo_2C-CTAB is electronegative. Moreover, considering the weak signal of C-Mo-Br species in Fig. 4b, it can be concluded that the hydrothermal etching strategy in this paper made an instability of -Br or -Cl, which were easily replaced by -O or -OH. Therefore, the surface of Mo_2C-CTAB is mainly terminated by -O and a little -OH/Br/Cl, and the Fermi level of Mo_2C-CTAB can be approximatively regarded as 1.09 V *vs*. NHE.

Tab. S4 Comparison of the photocatalytic H_2 production performance under visible-light of CZS/Mo_2C and other state-of-the-art CZS-based photocatalysts previously reported.

Photocatalyst	Catalyst amount (mg)	Sacrificial agent	Optimum co-catalyst loading	Light intensity (mW/cm^2)	H_2-rate ($mmol\ g^{-1}\ h^{-1}$)	Ref.
CZS/Mo_2C	20	Lactic acid	20 wt.%	80	44.19	This work
CZS/Ti_3C_2	10	Na_2SO_3/Na_2S	1 wt.%	N/A	15.0	7
CdS/Ti_3C_2	20	Lactic acid	2.5 wt.%	80	14.3	8
MoS_2/Ti_3C_2	30	Methanol	30 wt.%	N/A	6.1	9
Nb_2C/Nb_2O_5/C	40	Methanol	51 mol.%	120	0.007	10
CdS/Nb_2C	10	Lactic acid	15 wt.%	N/A	5.0	11
g-C_3N_4/Ti_2C	50	Triethanolamine	0.4 wt.%	N/A	0.95	12
CZS/g-C_3N_4	20	Na_2SO_3/Na_2S	32 wt.%	1.5	33.4	13
CZS/$CoFe_2O_4$	100	Na_2SO_3/Na_2S	7 wt.%	48.9	0.35	14
CZS/Ni_2P	50	Na_2SO_3/Na_2S	0.3 mol%	100	41.2	15
CZS/$SrTiO_3$	50	Na_2SO_3/Na_2S	N/A	150	25.0	16
CZS/NiB	6.6	Lactic acid	15 wt.%	N/A	8.1	17
CZS/La	N/A	Na_2SO_3/Na_2S	2 wt.%	N/A	1.39	18
CZS-P/Pt-PdS	10	Na_2SO_3/Na_2S	N/A	100	7.1	19

Supplementary References

1 Z. H. Han, G. Chen, C. M. Li, Y. G. Yu and Y. S. Zhou, *J. Mater. Chem. A*, 2015, **3**, 1696-1702.

2 X. Zhang, Z. Zhao, W. Zhang, G. Zhang, D. Qu, X. Miao, S. Sun and Z. Sun, *Small*, 2016, **12**, 793-801.

3 N. V. Tzenov and M. W. Barsoum, *J. Am. Ceram. Soc.*, 2000, **83**, 825-832.

4 G. Barbero and I. Lelidis, *Phys. Chem. Chem. Phys.*, 2017, **19**, 24934-24944.

5 S. Jin, Z. Shi, H. Jing, L. Wang, Q. Hu, D. Chen, N. Li and A. Zhou, *ACS Appl. Energy Mater.*, 2021, **4**, 12754-12766.

6 J. Halim, K. M. Cook, M. Naguib, P. Eklund, Y. Gogotsi, J. Rosen and M. W. Barsoum, *Appl. Surf. Sci.*, 2016, **362**, 406-417.

7 S. Zheng, S. Peng, Z. Wang, J. Huang, X. Luo, L. Han and X. Li, *Ceram. Int.*, 2021, **47**, 28304-28311.

8 J. R. Ran, G. P. Gao, F. T. Li, T. Y. Ma, A. J. Du and S. Z. Qiao, *Nat. Commun.*, 2017, **8**, 13907.

9 J. Zhang, C. Xing and F. Shi, *Int. J. Hydrogen. Energ.*, 2020, **45**, 6291-6301.

10 T. M. Su, R. Peng, Z. D. Hood, M. Naguib, I. N. Ivanov, J. K. Keum, Z. Z. Qin, Z. H. Guo and Z. L. Wu, *Chemsuschem*, 2018, **11**, 688-699.

11 J. Huang, M. Wang, X. Zhang, J. Tao, L. Lu, G. Qiao and G. Liu, *J. Alloy. Compd.*, 2022, **923**, 166256.

12 M. M. Shao, Y. F. Shao, J. W. Chai, Y. J. Qu, M. Y. Yang, Z. L. Wang, M. Yang, W. F. Ip, C. T. Kwok, X. Q. Shi, Z. G. Lu, S. J. Wang, X. S. Wang and H. Pan, *J. Mater. Chem. A*, 2017, **5**, 16748-16756.

13 L. Yao, D. Wei, Y. Ni, D. Yan and C. Hu, *Nano Energy*, 2016, **26**, 248-256.

14 Z. Shao, T. Zeng, Y. He, D. Zhang and X. Pu, *Chem. Eng. J.*, 2019, **359**, 485-495.

15 T. Yu, Y. Si, Z. Lv, K. Wang, Q. Zhang, X. Liu, G. Wang, G. Xie and L. Jiang, *Int. J. Hydrogen. Energ.*, 2019, **44**, 31832-31840.

16 T. Yu, Z. Lv, K. Wang, K. Sun, X. Liu, G. Wang, L. Jiang and G. Xie, *J. Power*

Sources, 2019, **438**, 227014.

17 L. Song, S. Zhang, D. Liu, S. Sun and J. Wei, *Int. J. Hydrogen. Energ*, 2020, **45**, 8234-8242.

18 Y. G. Yu, G. Chen, L. X. Hao, Y. S. Zhou, Y. Wang, J. Pei, J. X. Sun and Z. H. Han, *Chem. Commun.*, 2013, **49**, 10142-10144.

19 K. Khan, X. Tao, M. Shi, B. Zeng, Z. Feng, C. Li and R. Li, *Adv. Funct. Mater.*, 2020, **30**, 2003731.